Research Article | Vol. 8, No. 2 | 1 Feb 2017 | BIOMEDICAL OPTICS EXPRESS 764
Biomedical Optics EXPRESS

Clinically compatible flexible wide-field multi-color fluorescence endoscopy with a porcine colon model

GYUGNSEOK OH,[1] YOUNGRONG PARK,[2] SU WOONG YOO,[3] SOONJOO HWANG,[3] ALEXEY V. DAN CHIN-YU,[4] YEON-MI RYU,[5] SANG-YEOB KIM,[5,6] EUN-JU DO,[5] KI HEAN KIM,[7] SUNGJEE KIM,[2] SEUNG-JAE MYUNG,[5,8] AND EUIHEON CHUNG[1,3,*]

[1]*School of Mechanical Engineering, Gwangju Institute of Science and Technology, Gwangju, South Korea*
[2]*Department of Chemistry, Pohang University of Science and Technology, Pohang, South Korea*
[3]*Department of Biomedical Science and Engineering, Institute of Integrated Technology (IIT), Gwangju Institute of Science and Technology, Gwangju, South Korea*
[4]*Hyunjoo In-Tech, Suite 1901, Daeryung Poster Tower 1, Seoul, South Korea*
[5]*Asan Institute for Life Sciences, Asan Medical Center, Seoul, South Korea*
[6]*Department of Convergence Medicine, University of Ulsan College of Medicine, Seoul, South Korea*
[7]*Department of Mechanical Engineering, Pohang University of Science and Technology, Pohang, South Korea*
[8]*Department of Gastroenterology and Convergence Medicine, Asan Medical Center, University of Ulsan College of Medicine, Seoul, South Korea*
[*]*ogong50@gist.ac.kr*

Abstract: Early detection of structural or molecular changes in dysplastic epithelial tissues is crucial for cancer screening and surveillance. Multi-targeting molecular endoscopic fluorescence imaging may improve noninvasive detection of precancerous lesions in the colon. Here, we report the first clinically compatible, wide-field-of-view, multi-color fluorescence endoscopy with a leached fiber bundle scope using a porcine model. A porcine colon model that resembles the human colon is used for the detection of surrogate tumors composed of multiple biocompatible fluorophores (FITC, ICG, and heavy metal-free quantum dots (hfQDs)). With an *ex vivo* porcine colon tumor model, molecular imaging with hfQDs conjugated with MMP14 antibody was achieved by spraying molecular probes on a mucosa layer that contains xenograft tumors. With an *in vivo* porcine colon embedded with surrogate tumors, target-to-background ratios of 3.36 ± 0.43, 2.70 ± 0.72, and 2.10 ± 0.13 were achieved for FITC, ICG, and hfQD probes, respectively. This promising endoscopic technology with molecular contrast shows the capacity to reveal hidden tumors and guide treatment strategy decisions.

OCIS codes: (110.0110) Imaging systems; (170.4580) Optical diagnostics for medicine; (170.2150) Endoscopic imaging.

References and links

1. S. F. Pasha, J. A. Leighton, A. Das, M. E. Harrison, S. R. Gurudu, F. C. Ramirez, D. E. Fleischer, and V. K. Sharma, "Comparison of the yield and miss rate of narrow band imaging and white light endoscopy in patients undergoing screening or surveillance colonoscopy: a meta-analysis," Am. J. Gastroenterol. **107**(3), 363–371 (2012).
2. Sturm, M.B. and T.D. Wang," Emerging optical methods for surveillance of Barrett's oesophagus," Gut, gutjnl-2013–306706 (2015).
3. G. Oh, E. Chung, and S. H. Yun, "Optical fibers for high-resolution in vivo microendoscopic fluorescence imaging," Opt. Fiber Technol. **19**(6), 760–771 (2013).
4. G. Oh, S. W. Yoo, Y. Jung, Y.-M. Ryu, Y. Park, S.-Y. Kim, K. H. Kim, S. Kim, S.-J. Myung, and E. Chung, "Intravital imaging of mouse colonic adenoma using MMP-based molecular probes with multi-channel fluorescence endoscopy," Biomed. Opt. Express **5**(5), 1677–1689 (2014).

#281532 http://dx.doi.org/10.1364/BOE.8.000764
Journal © 2017 Received 25 Nov 2016; revised 3 Jan 2017; accepted 3 Jan 2017; published 10 Jan 2017

Biomedical Optics EXPRESS

5. R. Weissleder, "Molecular imaging in cancer," Science **312**(5777), 1168–1171 (2006).
6. J. T. Elliott, A. V. Dsouza, S. C. Davis, J. D. Olson, K. D. Paulsen, D. W. Roberts, and B. W. Pogue, "Review of fluorescence guided surgery visualization and overlay techniques," Biomed. Opt. Express **6**(10), 3765–3782 (2015).
7. S. S. Chauhan, B. K. Abu Dayyeh, Y. M. Bhat, K. T. Gottlieb, J. H. Hwang, S. Komanduri, V. Konda, S. K. Lo, M. A. Manfredi, J. T. Maple, F. M. Murad, U. D. Siddiqui, S. Banerjee, and M. B. Wallace; ASGE Technology Committee, "Confocal laser endomicroscopy," Gastrointest. Endosc. **80**(6), 928–938 (2014).
8. C. L. Zavaleta, E. Garai, J. T. Liu, S. Sensarn, M. J. Mandella, D. Van de Sompel, S. Friedland, J. Van Dam, C. H. Contag, and S. S. Gambhir, "A Raman-based endoscopic strategy for multiplexed molecular imaging," Proc. Natl. Acad. Sci. U.S.A. **110**(25), E2288–E2297 (2013).
9. E. Garai, S. Sensarn, C. L. Zavaleta, N. O. Loewke, S. Rogalla, M. J. Mandella, S. A. Felt, S. Friedland, J. T. Liu, S. S. Gambhir, and C. H. Contag, "A real-time clinical endoscopic system for intraluminal, multiplexed imaging of surface-enhanced Raman scattering nanoparticles," PLoS One **10**(4), e0123185 (2015).
10. Choi, J. and D. Drozek," Detection of looping during colonoscopy using bending sensors," TOMDJ **5**(1) (2013).
11. M. Hughes, P. Giataganas, and G.-Z. Yang, "Color reflectance fiber bundle endomicroscopy without back-reflections," J. Biomed. Opt. **19**(3), 030501 (2014).
12. T. Kimura, N. Muguruma, S. Ito, S. Okamura, Y. Imoto, H. Miyamoto, M. Kaji, and E. Kudo, "Infrared fluorescence endoscopy for the diagnosis of superficial gastric tumors," Gastrointest. Endosc. **66**(1), 37–43 (2007).
13. J. R. van der Vorst, M. Hutteman, K. N. Gaarenstroom, A. A. Peters, J. S. D. Mieog, B. E. Schaafsma, P. J. Kuppen, J. V. Frangioni, C. J. van de Velde, and A. L. Vahrmeijer, "Optimization of near-infrared fluorescent sentinel lymph node mapping in cervical cancer patients," Int. J. Gynecol. Cancer **21**(8), 1472–1478 (2011).
14. Sturm, M.B., B.P. Joshi, S. Lu, C. Piraka, S. Khondee, B.J. Elmunzer, R.S. Kwon, D.G. Beer, H.D. Appelman, and D.K. Turgeon, "Targeted imaging of esophageal neoplasia with a fluorescently labeled peptide: first-in-human results," Sci. Transl. Med. **5**, 184 (2013).
15. B. P. Joshi, X. Duan, R. S. Kwon, C. Piraka, B. J. Elmunzer, S. Lu, E. F. Rabinsky, D. G. Beer, H. D. Appelman, S. R. Owens, R. Kuick, N. Doguchi, D. K. Turgeon, and T. D. Wang, "Multimodal endoscope can quantify wide-field fluorescence detection of Barrett's neoplasia," Endoscopy **48**(2), A1–A13 (2016).
16. G. M. van Dam, G. Themelis, L. M. Crane, N. J. Harlaar, R. G. Pleijhuis, W. Kelder, A. Sarantopoulos, J. S. de Jong, H. J. Arts, A. G. van der Zee, J. Bart, P. S. Low, and V. Ntziachristos, "Intraoperative tumor-specific fluorescence imaging in ovarian cancer by folate receptor-α targeting: first in-human results," Nat. Med. **17**(10), 1315–1319 (2011).
17. C. Lim, E. Vibert, D. Azoulay, C. Salloum, T. Ishizawa, R. Yoshioka, Y. Mise, Y. Sakamoto, T. Aoki, Y. Sugawara, K. Hasegawa, and N. Kokudo, "Indocyanine green fluorescence imaging in the surgical management of liver cancers: current facts and future implications," J. Visc. Surg. **151**(2), 117–124 (2014).
18. Y. Park, Y.-M. Ryu, Y. Jung, T. Wang, Y. Baek, Y. Yoon, S. M. Bae, J. Park, S. Hwang, J. Kim, E. J. Do, S. Y. Kim, E. Chung, K. H. Kim, S. Kim, and S. J. Myung, "Spraying quantum dot conjugates in the colon of live animals enabled rapid and multiplex cancer diagnosis using endoscopy," ACS Nano **8**(9), 8896–8910 (2014).
19. X. Kang, L. Huang, Y. Yang, and D. Pan, "Scaling up the aqueous synthesis of visible light emitting multinary AgInS2/ZnS core/shell quantum dots," J. Phys. Chem. C **119**(14), 7933–7940 (2015).
20. A. Shamirian, O. Appelbe, Q. Zhang, B. Ganesh, S. J. Kron, and P. T. Snee, "A toolkit for bioimaging using near-infrared AgInS 2/ZnS quantum dots," J. Mater. Chem. B Mater. Biol. Med. **3**(41), 8188–8196 (2015).
21. L. Ye, K.-T. Yong, L. Liu, I. Roy, R. Hu, J. Zhu, H. Cai, W.-C. Law, J. Liu, K. Wang, J. Liu, Y. Liu, Y. Hu, X. Zhang, M. T. Swihart, and P. N. Prasad, "A pilot study in non-human primates shows no adverse response to intravenous injection of quantum dots," Nat. Nanotechnol. **7**(7), 453–458 (2012).
22. P. Subramaniam, S. J. Lee, S. Shah, S. Patel, V. Starovoytov, and K. B. Lee, "Generation of a library of non-toxic quantum dots for cellular imaging and siRNA delivery," Adv. Mater. **24**(29), 4014–4019 (2012).
23. C. Nossol, A. Barta-Böszörményi, S. Kahlert, W. Zuschratter, H. Faber-Zuschratter, N. Reinhardt, S. Ponsuksili, K. Wimmers, A.-K. Diesing, and H.-J. Rothkötter, "Comparing Two Intestinal Porcine Epithelial Cell Lines (IPECs): Morphological Differentiation, Function and Metabolism," PLoS One **10**(7), e0132323 (2015).
24. J. K. Patterson, X. G. Lei, and D. D. Miller, "The pig as an experimental model for elucidating the mechanisms governing dietary influence on mineral absorption," Exp. Biol. Med. (Maywood) **233**(6), 651–664 (2008).
25. ANSftSUo, L.," American national standard for the safe use of lasers," American National Standards Institute. ANSIZ136. New York, NY: American National Standards Institute (2007)
26. N. Sengupta and T. T. MacDonald, "The role of matrix metalloproteinases in stromal/epithelial interactions in the gut," Physiology (Bethesda) **22**(6), 401–409 (2007).
27. T. Torimoto, S. Ogawa, T. Adachi, T. Kameyama, K. Okazaki, T. Shibayama, A. Kudo, and S. Kuwabata, "Remarkable photoluminescence enhancement of ZnS-AgInS2 solid solution nanoparticles by post-synthesis treatment," Chem. Commun. (Camb.) **46**(12), 2082–2084 (2010).
28. J. Park, J. Nam, N. Won, H. Jin, S. Jung, S. Jung, S. H. Cho, and S. Kim, "Compact and Stable Quantum Dots with Positive, Negative, or Zwitterionic Surface: Specific Cell Interactions and Non-Specific Adsorptions by the Surface Charges," Adv. Funct. Mater. **21**(9), 1558–1566 (2011).
29. J. Decock, S. Thirkettle, L. Wagstaff, and D. R. Edwards, "Matrix metalloproteinases: protective roles in cancer," J. Cell. Mol. Med. **15**(6), 1254–1265 (2011).

Biomedical Optics EXPRESS

30. C.-Y. Lin, C.-H. Lee, C.-C. Huang, S.-T. Lee, H.-R. Guo, and S.-B. Su, "Impact of high glucose on metastasis of colon cancer cells," World J. Gastroenterol. **21**(7), 2047–2057 (2015).
31. Q. Zhang, G. Widmer, and S. Tzipori, "A pig model of the human gastrointestinal tract," Gut Microbes **4**(3), 193–200 (2013).
32. W. Kang, H. Wang, Z. Wang, M. W. Jenkins, G. A. Isenberg, A. Chak, and A. M. Rollins, "Motion artifacts associated with in vivo endoscopic OCT images of the esophagus," Opt. Express **19**(21), 20722–20735 (2011).
33. R. J. Cooper, J. Selb, L. Gagnon, D. Phillip, H. W. Schytz, H. K. Iversen, M. Ashina, and D. A. Boas, "A systematic comparison of motion artifact correction techniques for functional near-infrared spectroscopy," Front. Neurosci. **6**, 147 (2012).
34. S. Lee, C. Vinegoni, M. Sebas, and R. Weissleder, "Automated motion artifact removal for intravital microscopy, without a priori information," Sci. Rep. **4**, 4507 (2014).
35. M. A. Funovics, H. Alencar, X. Montet, R. Weissleder, and U. Mahmood, "Simultaneous fluorescence imaging of protease expression and vascularity during murine colonoscopy for colonic lesion characterization," Gastrointest. Endosc. **64**(4), 589–597 (2006).
36. J. Mendelsohn and J. Baselga, "Status of epidermal growth factor receptor antagonists in the biology and treatment of cancer," J. Clin. Oncol. **21**(14), 2787–2799 (2003).
37. E. M. Sevick-Muraca, "Translation of near-infrared fluorescence imaging technologies: emerging clinical applications," Annu. Rev. Med. **63**(1), 217–231 (2012).
38. Scheuer, W., G.M. van Dam, M. Dobosz, M. Schwaiger, and V. Ntziachristos, "Drug-based optical agents: infiltrating clinics at lower risk," Sci. Transl. Med. **4**, 134 (2012).
39. L. Barault, N. Veyrie, V. Jooste, D. Lecorre, C. Chapusot, J. M. Ferraz, A. Lièvre, M. Cortet, A. M. Bouvier, P. Rat, P. Roignot, J. Faivre, P. Laurent-Puig, and F. Piard, "Mutations in the RAS-MAPK, PI (3) K (phosphatidylinositol-3-OH kinase) signaling network correlate with poor survival in a population-based series of colon cancers," Int. J. Cancer **122**(10), 2255–2259 (2008).

1. Introduction

Colon cancer is one of the most common malignancies in many developed countries. Early diagnosis of precancerous lesions in the colon with endoscopy has been shown to reduce mortality. Conventional endoscopy can transmit light deep inside the gastrointestinal (GI) tract for the visualization of precancerous lesions. Endoscopic imaging is critical to observing precancerous lesions because the lesions are heterogeneous in shape, often flat, and small. However, the missing rate of detecting smaller-sized polyps can go up to 27% [1]. Moreover, conventional white light endoscopy cannot provide information on molecular changes and thus, may result in unnecessary biopsies for further diagnosis. There have been various optical endoscopic imaging modalities including auto-fluorescence imaging, chromo-endoscopy, narrow-band imaging, and optical coherence tomography [2]. However, endoscopic imaging modalities based on structural changes cannot provide sufficient information for rapid and accurate screening due to the nonspecific background from the tissue surface [2]. Among other imaging methods, molecular endoscopic imaging with wide-field of view is an emerging modality to screen precancerous lesions in real-time, based on molecular signatures, when used in combination with clinical endoscopy [3]. Oftentimes, precancerous lesions overexpress certain enzymes or receptors in altered colonic mucosa or epithelial cell surfaces. The molecular contrast between normal and tumor cells may provide an efficient method of tumor detection with fluorescently-labeled molecular targets [4]. As the most novel imaging method in medicine, molecular imaging modalities potentially allow clinicians to locate hidden lesions by visualizing molecular characteristics [5, 6].

In clinics, confocal endoscopic methods such as fluorescence endomicroscopy (Cellvizio, Mauna Kea Technology, Paris, France) provide cellular-resolution images with fluorophores [7]. However, the confocal laser endoscope has a small field of view (several hundreds of microns) with only contact mode. Raman-based endoscopy can detect very low concentrations (~pM) [8] with noncontact mode. However, it suffers from long image acquisition time [9]. Although the resolution and sensitivity are lower in our device than confocal and Raman-based endoscopes, our endoscope is able to acquire clinically-relevant surface images quickly, making it suitable as a screening device.

The optical fiber bundle is a fundamental element for implementing endoscopy for flexible maneuvering along the curved lumen of animal or human gastrointestinal tracts [3]. The leached fiber bundle type is manufactured by laying up rigid, double-clad core rods in a

Biomedical Optics EXPRESS

closely packed array, such that any particular core occupies the same position in the matrix at both ends of the bundle. Over the whole bundle, the outer layer of cladding is removed from each core by acid leaching, separating the fibers, and rendering the bundle extremely flexible. While the minimum bending radius (MBR) of conventional imaging fiber bundles with 1 mm outer diameter (Fujikura LTd., Tokyo, Japan) is 100 mm, a leached fiber bundle with the same diameter can reduce the MBR down to 25 mm. Leached fiber bundles are suitable for compatibility with clinical endoscopes because the MBR of the imaging scope is not larger than 50.8 mm [10]. To insert into the biopsy channel of commercial clinical endoscopes, we constructed our probe using a leached fiber bundle [11].

Efficient tumor detection can be achieved with fluorescently labeled organic fluorophores (fluorescein isothiocyanate, FITC, and indocyanine green, ICG) or inorganic fluorophores (i.e., quantum dots, QDs) potentially allowing clinicians to spot invisible tumor lesions. ICG and FITC are well-known FDA-approved fluorophores for human use [12, 13], and have been used as a contrast agent for lesion detection in clinics. For targeted imaging of esophageal neoplasia with FITC-labeled peptides in humans, the range of concentration is 100 to 1000 μM [14]. Moreover, some researchers have used the ASY-FITC peptide with 100 μM concentration to detect Barrett's neoplasia using their endoscopic systems in patients [15]. In another study, FR-α-targeted agent folate-FITC was found to be safe and offering specific and sensitive identification of ovarian tumor tissues during surgery in patients with ovarian cancer [16]. ICG is a fluorescent marker that is excited at a wavelength between 600 and 900 nm to emit maximum fluorescence at 810 nm in water and 830 nm in blood. ICG was particularly used in previous studies [13, 17] to improve lymph node mapping and enhance tumor contrast. Infrared fluorescence endoscopy with ICG has been used to observe GI vascular structure and may provide precancerous information [12].

In practice, many tumors express multiple cell surface and proteomic markers. Therefore, simultaneous multi-fluorophore imaging of numerous molecular targets is important for accurate cancer diagnosis. In addition to their resistance to photobleaching, quantum dots (QDs) are ideal for multispectral imaging where different types of cells or tissues can be imaged simultaneously by labeling with distinct QDs at different wavelengths. Recently, specific molecular targeting with mouse colonic tumor and human colon adenoma was performed with QD-conjugates that contain heavy metal [18]. However, the inherent potential toxicity prevents cadmium- or lead-based QDs from being used for clinical imaging. Therefore, it is vital to develop other types of QDs with reduced toxicity. Several QD toxicity studies have addressed and reduced in vivo toxicity by coating the cadmium-based core with another material [19, 20]. However, a study with nonhuman primates revealed that most of the initial dose of cadmium still remained in the liver, spleen, and kidneys 90 days after injection [21]. This means that the clearance of QDs can be quite slow, suggesting that longer-term studies will be required to determine the ultimate fate of these heavy metals and the impact of their remnants on the body. Ternary group I-III-VI QDs, such as $AgInS_2$ QDs, are deemed better candidates as they contain no highly toxic elements. The $AgInS_2$/ZnS QDs showed significantly improved biocompatibility (less cytotoxic, 95% cell viability) in both brain tumor cells and stem cells at high concentrations in comparison with that of the CdSe/ZnS QDs, which were found to be cytotoxic at even low concentrations [22]. Thus, we used heavy metal-free $AgInS_2$/ZnS QDs in this study.

The porcine model is a suitable model for studying intestinal development or disease and pretest in screening of lesions due to its physiological resemblance to the human colon in terms of geometry and size [23]. It has been used as an animal model to investigate human gastrointestinal diseases because human intestinal samples are limited and valuable [24]. Our endoscopic system was used with a clinical endoscope to screen polyps in the porcine colon.

In this study, we describe a home-built, flexible, wide-field molecular fluorescence endoscope compatible with clinical endoscopes and its validation by in vivo experiments on a porcine colon. Furthermore, we use biocompatible fluorophores including heavy metal-free

Biomedical Optics EXPRESS

QDs, which may be useable in future clinical applications. The endoscopic imaging system was tested and evaluated in a pilot study on a porcine colon with acutely formed fluorescent surrogate tumors. To assess its feasibility in clinical settings, we used our system in conjunction with a clinical sigmoidoscope.

2. Materials and methods

Endoscopy imaging system

We have created a small, flexible, fiber-optic, multi-color fluorescence endoscopic imaging probe, designed for clinical compatibility to comprehensively image the luminal surface of a colon in noncontact mode. The endoscopic system consists of an imaging scope, excitation light sources (473 nm and 785 nm), white light-emitting diode (LED), and a detection unit. The constructional features and the workings of the system are described next. Multi-color fluorescence imaging is realized by a filter wheel at the emission optical path, and illumination is delivered via adjacent multimode fibers. To excite multiple fluorophores sequentially, the light from the 473 nm laser (SDL-473-300T, Shanghai Dream Lasers Technology) and the 785 nm laser (MDL-III-785-1W, Shanghai Dream Lasers Technology) are coupled onto multimode fibers (NA 0.55, SCHOTT AG) using an achromatic VIS-NIR-coated lens with an effective focal length (EFL) of 18 mm. The reflected and emitted fluorescence light are collected via a micro-lens and relayed back to the optical path by the image scope (Fig. 1(a)). The light passes through two achromatic lenses with EFLs of 10 and 40 mm (Edmund Optics), an emission filter wheel (630 nm BPF, 525 nm BPF and 808 nm LP, Semrock), and a dichroic mirror. The reflectance image is captured by a charge-coupled device (CCD) camera (QIClick, QImaging). Fluorescence images are acquired sequentially with another CCD camera (PCO pixelfly, PCO AG), simultaneously.

Biomedical Optics EXPRESS

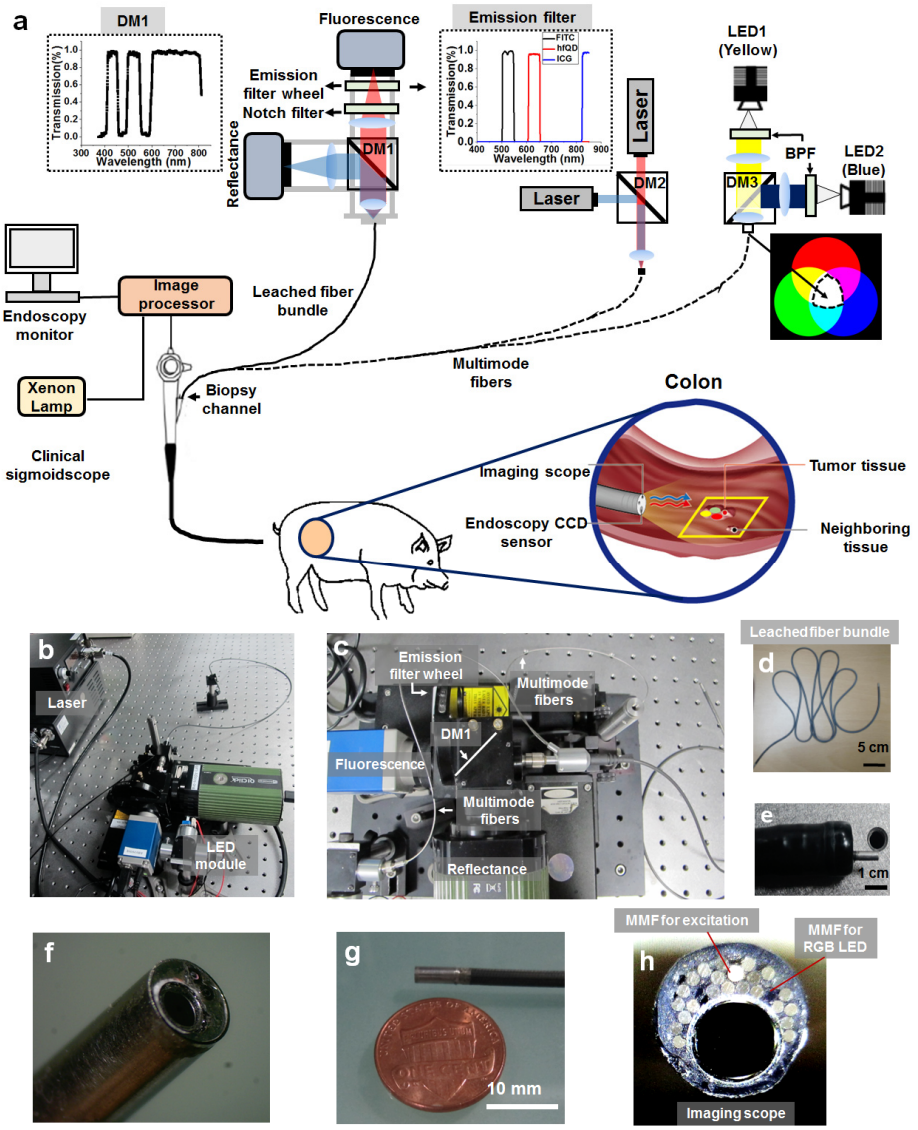

Fig. 1. Configuration of the clinically-compatible flexible wide-field multi-color fluorescence endoscope system. (a) Schematic of multi-color fluorescence endoscope designed to be inserted through the biopsy channel (diameter: 3.2 mm) of a clinical sigmoidoscope. The system is comprised of two detection channels: reflectance and fluorescence. Multiple-channel fluorescence imaging is obtained by the rotating filter wheel in front of the fluorescence camera detector. (b–c) Photographs of the imaging device and system. (c) An enlarged view of the detection part in the endoscopic system. (d) Photograph of highly flexible leached fiber bundle used for home-made probes. Note that the leached fiber bundle in (a) is not visible in (c). (e) Photograph of combined imaging scope and sigmoidoscope. (f–g) Close-up photograph of the distal end of the imaging scope. The scope was enclosed and sealed within an aluminum sheath. The magnified imaging scope shows a leached fiber bundle and multimode fibers for delivering excitation light and white light (from LEDs). (h) Frontal view of the distal end of the imaging scope. Acronyms are defined as follows: (LED: Light-emitting diode, DM: Dichroic mirror, MMF: Multi-mode fiber, BPF: Band-pass filter, RGB: Red green blue).

The imaging scope consists of an imaging scope with a micro-lens attached on a leached fiber bundle (O.D: 1.0 mm, Cat.1537357, SCHOTT AG) and multimode fibers for delivering excitation light from two laser light sources at 473 nm and 785 nm wavelengths. The output

Biomedical Optics EXPRESS

excitation power was approximately 10 mW on the tissue, which is less than the American National Standards Institute's (ANSI) maximum permissible skin exposure limit set out for laser beams [25]. To provide cool white light with a color temperature of 5,000–5,500 K, a balanced combination of yellow- and blue-emitting LEDs (Ultrabright, Cree Inc., Durham, NC) with band-pass filters (475/25 nm and 575/25 nm) was used for the white light LED module, and the combined white light is delivered onto the multimode fibers. Each LED was driven continually by a driver module (MicroPuck, LEDdynamics Inc., Randolph, VT). A micro-lens (CAT #5337-750, precision optics corporation, Gardner, MA) cemented at the distal end of the leached fiber bundle, protected with stainless steel mesh, and covered with PTFE (Teflon) tubing provided a field of view of approximately 64 cm^2 in front of the specimen at a distance of 3 cm (Fig. 1(d)). The outer diameter of the imaging scope is 2.8 mm, enabling the scope to pass through the biopsy channel of a clinical sigmoidoscope (DF200S, Olympus) with an inner diameter of 3.2 mm (Fig. 1(f)). The endoscopic system can acquire an image of a positive 1951 USAF resolution target at group 3/element 6 which corresponds to a lateral resolution of 70.1 μm.

Characterization of heavy metal-free QDs conjugated with MMP14 antibody

Matrix metalloproteinases-14 (MMP14) is a membrane-associated enzyme associated with cancer invasion and metastasis [26]. Overexpression of MMP14 is expected at the peripherals of tumors nearby luminal surfaces. MMP14 antibodies (Abs) were conjugated with red light emitting $AgInS_2$/ZnS (core/shell) QDs, which are heavy metal-free QDs (hfQDs). Red-color-emitting hfQDs were synthesized using procedures previously described [27]. The absorption and fluorescence profiles of the nanoparticle are shown in Fig. 2(a), where the emission peaks can be found at 660 nm. The quantum efficiency of hfQD is 42.8%. The surface of the QDs was co-decorated with a zwitterionic ligand and a ligand bearing carboxylic acid [28]. The carboxylic acids were used for conjugation with the MMP14 Abs. To test the biocompatibility of hfQDs for use as imaging probes in vitro, a cytotoxicity assay was carried out in cancer cells. The concentration-dependent cytotoxicity of the water-soluble hfQDs was assessed in cancer cells for a cell proliferation assay (Fig. 2(c)). Cell viability using the QDs is higher than using CdSe/ZnS QDs in human brain tumor cells (U87 glioblastoma cell line) and human bone-marrow-derived mesenchymal stem cells (hMSCs) [22]. Human colon cancer cells (HCT116) were chosen as an MMP-expressed group and human breast cancer cells (MCF7) for the negative control. When co-incubated, MMP-QDs showed cell-specific labeling for the HCT116 cells, whereas no noticeable signal could be found for the MCF7 cells (Fig. 2(d)).

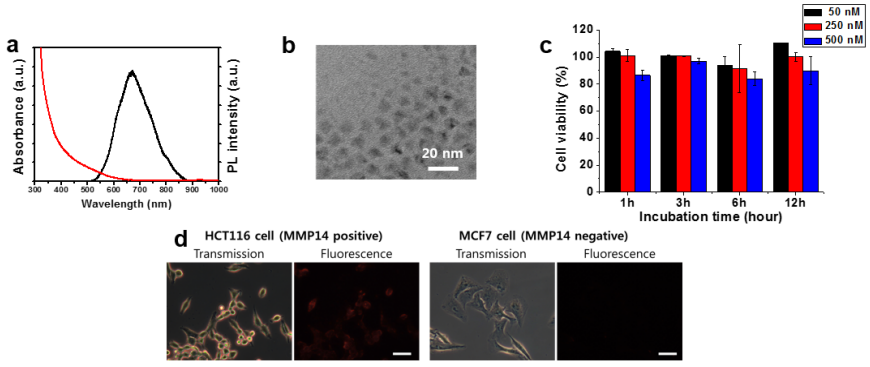

Fig. 2. (a) Absorption and fluorescence profiles of the hfQDs. (b) Transmission electron microscopic image of the hfQDs. (c) Cytotoxicity measurements of HCT116 cells with hfQDs. For QDs toxicity, cells were treated with 50, 250, and 500 nM of quantum dots for 1–12 h at 37 °C. After the incubation, cell viability was measured by CCK-8 assay. (d) Fluorescence imaging with MMP14-QDs in HCT116 and MCF7 cells. Scale bar = 50 μm.

Biomedical Optics EXPRESS

Targeted molecular imaging of tumors with MMP14Ab-heavy metal-free QD in ex vivo porcine colons

To investigate the applicability of biocompatible MMP14 Ab-hfQD probes in the spraying and washing method [18], fresh tumor tissue was harvested from a subcutaneous mouse CT26 (colon carcinoma cell line) xenograft model, and embedded in an ex vivo porcine colon tissue. The fresh tumor tissues were sprayed by 300 nM MMP14 Ab-hfQD probes in PBS solution with only PBS solution used as control. The tissues were thereafter incubated for 30 min, and washed with PBS buffer three times prior to imaging. From this in vitro cytotoxicity testing with HCT116 cells, we assumed the hfQD concentration of less than 500 nM as innocuous and used for the subsequent experiments

In vivo multiple fluorescence surrogate tumor imaging in porcine colon

The performance of the multi-color fluorescence endoscopic imaging system in vivo was validated in a porcine colon (Yorkshire pig) with 30 kg body weight that resembles the human colon. We first anesthetized the pig with 4% isoflurane for induction. We maintained anesthesia with 1.5%–2.0% isoflurane supplied through endotracheal intubation during imaging after removing stools in the colon. We tested in vivo multi-color fluorescence imaging capabilities after creating surrogate tumors made of multiple fluorophores. In the colon tissue, a simple injection of three probes (FITC, hfQDs, and ICG) into the colonic tissue using a clinical injection needle (NM-400U-0423, Olympus) allowed fluorescence imaging immediately after injection. The animal studies were performed under the supervision of the Institutional Animal Care and Use Committee of the Asan Medical Center by the approved institutional protocols (Fig. 3).

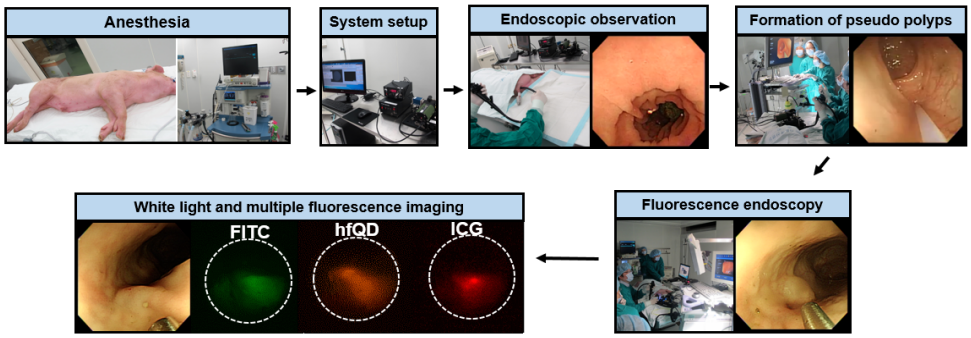

Fig. 3. In vivo fluorescence endoscopic imaging protocol in porcine colon. Prior to the imaging, a 30 kg Yorkshire pig was anesthetized with isoflurane (1.5%–2.0%) through endotracheal intubation and the multi-color fluorescence endoscope was set. Next, the observation of the porcine colon using the clinical sigmoidoscope was performed to remove any existing stool with PBS solution. Prior to fluorescence imaging, a mixture of fluorophores was injected into the colonic wall to form surrogate tumors using the clinical injector.

In vivo fluorescence imaging of surrogate tumors with colon cancer cells in porcine colon

Colon 38 SL4 cell line, a metastatic cell line of colon cancer was cultured with DMEM/F12 (Life Technologies; containing L-Glutamine, 2.438 g/L sodium Bicarbonate), 10% fetal bovine serum (FBS, Life Technologies), 1% penicillin streptomycin (Life Technologies; containing 10,000 units/mL penicillin, 10,000 μ g/mL streptomycin, and 25 μg/mL amphotericin B) as cell medium. The quantity of cells was 14.75×10^6 cells/mL. The molecular fluorescence endoscope can detect fluorescence light in surrogate tumors after injecting SL4-DsRed cancer cells with 100 μL volume.

Biomedical Optics EXPRESS

3. Results

Ex vivo targeted fluorescence endoscopic imaging of syngeneic mouse tumors with MMP14Ab-heavy metal-free QDs in the porcine colon tissue

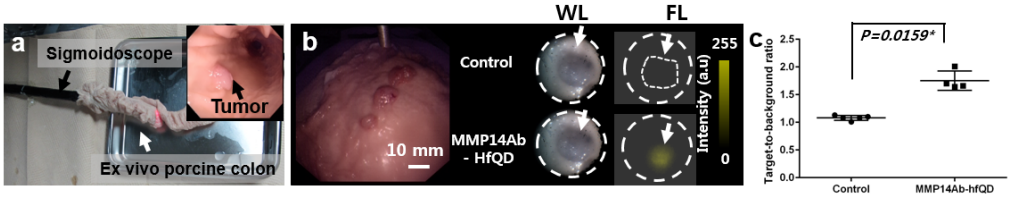

Fig. 4. Ex vivo tumor-targeted fluorescence image with MMP14Ab-hfQD probe in the porcine colon. (a) Experimental configuration. (b) Tumor-targeted fluorescence imaging using MMP14Ab-hfQD and PBS solution as control with grafted mouse tumors in the porcine colon. (c) Quantified TBR using PBS solution and MMP14ab-hfQD ex vivo with 1.08 ± 0.05 and 1.74 ± 0.06, respectively. $p < 0.05$ by unpaired t-test.

We first performed molecular fluorescence endoscopic imaging in ex vivo porcine colon tissue by spraying molecular probes (MMP14Ab-hfQDs) onto the target, a syngeneic mouse tumor tissue (Fig. 4). MMP participates in various physiological and pathological processes such as arthritis and tumor progression, and is known to be overexpressed in CT26 murine colon tumor [29, 30]. Ex vivo imaging shows the targeting of MMP14Ab-hfQDs to bind cell surface receptors with 30 min incubation time. The intrinsic background signal from the ex vivo porcine colon tissue did not interfere with fluorescence from the molecular target. The regions of interest (ROI) were placed in the tumor (S_t) and the adjacent tissue (S_n) and the ROI intensities were recorded in pixel intensity values between 0 and 255 with 8 bits. After obtaining mean signal intensities, the target-to-background ratio (TBR) was determined as S_t/S_n. Data are presented as means ± standard deviations, and each signal intensity value represents either tumor or neighboring tissue signal intensity after subtraction of background signal intensity (intrinsic camera noise). We measured the background signal using the same configuration except only blocking the excitation light. Tumor-specific fluorescence signals could be detected in tumor tissues using MMP14Ab-hfQDs where TBR was 1.74 ± 0.06. However, no fluorescence signal was detected in the tumor tissues using PBS solution. All fluorescence images were analyzed using the Image J software (National Institutes of Health, USA).

In vivo endoscopic imaging of multiple pseudo-polyps made of biocompatible fluorophores in the porcine colon

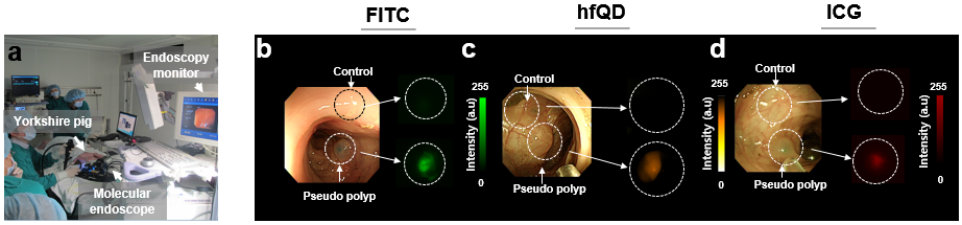

Fig. 5 In vivo fluorescence endoscopic imaging of surrogate tumors in the porcine colon with different fluorophores. (a) Experimental configuration. (b) Fluorescence imaging of surrogate tumors with FITC, ICG, and hfQDs in the porcine colon.

We tested the in vivo multi-color fluorescence imaging capability of our proposed system in the porcine colon after generation of surrogate tumors by injection of fluorophores (Fig. 5(a)). Each fluorophore with various concentrations of solution was injected into the porcine colonic tissue with 100 μL volume. PBS without fluorophores injected at a different site served as a control. Based on our empirical tests, we chose 1 mg/ml concentration (25.6 μM

Biomedical Optics EXPRESS

for FITC, 300 nM for hfQD and, 129 μM for ICG) for the feasibility of multi-color fluorescence endoscopic imaging in the porcine colon (Fig. 5(b)-5(d)). As the field of view of the sigmoidoscope and that of our endoscope were different, the fluorescence endoscopic probe was positioned closer to the surrogate tumors for imaging.

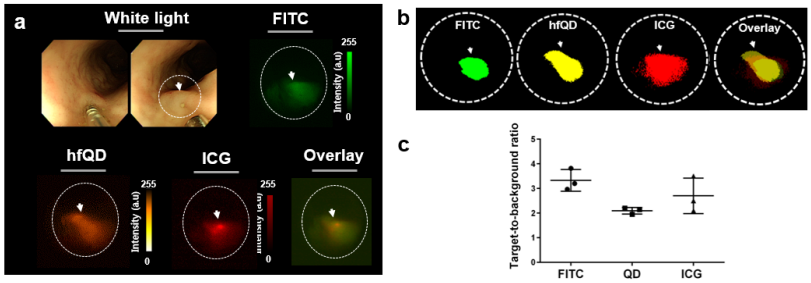

Fig. 6 In vivo multi-color fluorescence endoscopic imaging in the porcine colon. (a) (upper) Generation of a surrogate tumor with mixtures of multiple fluorophores. Fluorescence images of each dye were obtained with corresponding emission filters. (b) Threshold images of multiple fluorophores with the endoscope showing the distributions of each fluorophore and a merged image. (c) TBR of fluorophores in the surrogate tumor at the same concentration of 1 mg/ml.

For feasibility of multi-color fluorescence endoscopic imaging in vivo, three fluorophores with 1 mg/ml concentration were mixed to form a volume of 300 μL. Using a clinical injector needle, the mixture was injected into the porcine colon tissue. The endoscopic system can acquire each fluorescence signal with corresponding emission filters (Fig. 6(a)). The fluorescence signal in the adjacent tissue was defined as the background. The effect of each fluorophore with the same concentration on contrast was compared in terms of TBR. The TBR of each fluorescence imaging was 3.36 ± 0.43 for the FITC, 2.10 ± 0.13 for the QD, and 2.70 ± 0.72 for the ICG (Fig. 6(c)). These values are consistent with those of typical fluorescence endoscopy. The TBR is affected by tissue auto-fluorescence, the intensity and characterization of excitation light source, quantum yield, and camera quantum efficiency. In the system characterization studies, the strong light intensity was visible in the drop at a concentration of 1 mg/ml without a saturated image. Thus, we selected 1 mg/ml concentration for multi-color porcine colon detection. To estimate the polyp boundaries for each channel, we set threshold values that are the average of the maximum and the minimum values of each image (Fig. 6(b)) [4]. Although this simple approach works reasonably in the porcine colon, it may require more sophisticated threshold techniques. In the fluorescence imaging, the surrogate tumors with injected multiple fluorophores are clearly distinguishable from adjacent tissues in the porcine colon.

In vivo endoscopic imaging of a surrogate tumor composed of cancer cells in the porcine colon

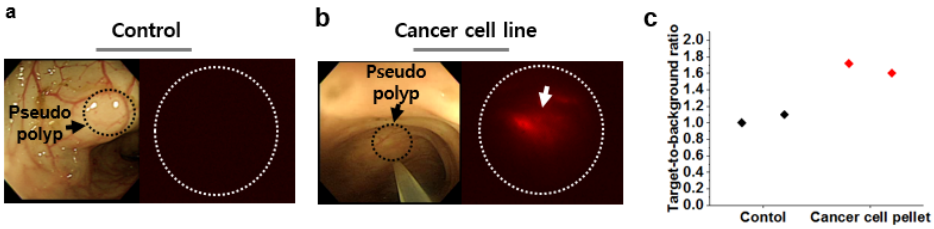

Fig. 7. Intra-vital in vivo fluorescence endoscopic imaging of SL4-DsRed cancer cell pellet in porcine colon. (a) Surrogate tumor imaging of PBS injection (control experiment). (b) Surrogate tumor fluorescence imaging of SL4-DsRed cancer cells. (c) Mean TBR value at the injection site of the colon cancer cells and control.

Biomedical Optics EXPRESS

For in vivo intra-vital targeted molecular imaging, we injected 100 μL of SL4-DsRed colon cancer cell pellets and the PBS control solution into the porcine colon tissue. Although the DsRed fluorophore has an excitation peak at 556 nm, it has a relatively broad excitation spectrum and could be excited with a 473 nm laser source and emission filter (611–649 nm). However, no signal was detected in the control injection site and adjacent colon tissue (Fig. 7). Mean TBR of each fluorescence image was 1.05 for the PBS solution and 1.66 for the SL4-DaRed cancer cell. The endoscopic system could detect surrogate tumors composed of cancer cells in the porcine colon in vivo.

4. Discussion and conclusion

Early detection of structural or molecular changes in dysplastic epithelial tissues may be crucial for improving patient care. Multi-color fluorescence endoscopic imaging with biocompatible fluorophores has the potential to improve the screening of tumors within the colon. In this work, we demonstrate clinically compatible, multi-color fluorescence imaging and the feasibility for in vivo assessment of surrogate tumors in porcine colons.

The porcine model is experimentally tractable and is an alternative model of the human GI tract. In addition, it offers significant advantages over rodent models for translational research [31]. However, experimental preparation takes longer, and imageable sites are limited due to the presence of stool in the porcine colon. We spent an average of approximately 3 h removing stool using PBS solution and injectors even after a two-day prefasting of the animal.

Our home-built endoscopic device was compatible with a clinical sigmoidoscope through the biopsy channel due to the use of a highly flexible leached fiber bundle instead of a conventional fiber bundle. Thus, leached fiber bundles are found suitable. They have several thousand fibers that are fixed short ferrules at either end of the bundle but are not bound together along the remainder of the length, with minimum bending radius of 25.0 mm.

The multi-color fluorescence endoscope can detect three fluorescence signals from FITC, hfQDs, and ICG at 100 ms exposure time (or 10 frames per second) for clinical translation.

A spraying method for tumor-targeted molecular imaging within the colon, as opposed to intravenous injection, can be applied to potentially minimize toxicity to patients. For porcine model studies, we chose a concentration of 1 mg/ml for each fluorophore (FITC, hfQDs, and ICG) solution. The endoscopic fluorescence imaging with FITC provided the highest TBR in the colon because of high quantum yield and high camera quantum efficiency at green wavelength. The hfQDs are potential molecular probes with sensitivity, good stability, and reduced phtobleaching compared to the other fluorophores. Another advantage of the hfQDs is the reduced harmful effects of toxic heavy metals, making them suitable for future clinical translation. However, the emission spectrum of hfQDs is still somewhat broader than that of cadmium-based QD nanoparticles. While we used the incubation time of 30 min for tumor detection based on our previous study [18] that is relatively long duration for human clinical studies, this incubation time could be reduced with further optimization.

In merged fluorescence images of the porcine colon, the fluorescence distribution could change due to time delays present in sequential image acquisition (~3 s) from manual control of filter wheel. Alternatively, one can reduce the sequential image acquisition time by use of the fast motorized filter wheel or simultaneous detection of different fluorescence with multiple cameras. Animal breathing and endoscopists' handling can generate movement artifacts. To resolve this problem in practice, motion artifact correction can be adapted [32, 33]. Some previous research show automated motion artifacts for intra-vital microscopy in small animal models [34]. For Moreover, simultaneous fluorescence endoscopic imaging for NIR channels can reduce movement artifacts [35]. Thus, heavy metal-free QDs at multiplexed NIR wavelength range can simultaneously provide imaging with high sensitivity and contrast without motion artifacts.

Biomedical Optics EXPRESS

Known molecular targets such as the epidermal growth factor (EGFR) that is known to be overexpressed in over 70% of human colorectal cancer [36], and others such as the human epidermal growth factor receptor2 (HER2), vascular endothelial growth factor (VEGF), and phosphoinositide 3-Kinase (PI3K) may be used to improve diagnostic sensitivity using the proposed endoscopic system with biocompatible fluorophores [37–39]. In addition, the fluorescence endoscopic imaging system has the potential to help investigate molecular mechanisms of colon cancer progression. In summary, we present the first clinically compatible, wide-field-of-view, multi-color fluorescence endoscope with leached fiber-bundle scope in a porcine colon model and demonstrate the feasibility with multiple biocompatible fluorophores towards clinical translation.

Funding

This work was supported by Biomedical Integrated Technology Research Project, GIST-Caltech Research Collaboration Project and the GIST Research Institute (GRI) provided by GIST in 2016, and by the Bio & Medical Technology Development program of the National Research Foundation (NRF) funded by the Korean government (MEST) (No. 2011-0019633, NRF-2016R1A2B4015381) and by the Ministry of Trade, Industry & Energy (MOTIE, Korea) under Industrial Technology Innovation Program. No. 10063408. 'Development of channel-inserted convergence smart endoscopic system based on multispectral fluorescence imaging for precise diagnosis of digestive diseases'.

Acknowledgment

The authors thank HYUNJOO IN-TECH for their technical support and Dr. Sung Wook Hwang, Dr. Sang Mun Bae and Ms. Jiyoung Shin from Asan Medical Center for their help during the animal experiment.